Journal of Thermal Analysis and Calorimetry, Vol. 83 (2006) 3, 657–668

THERMAL ANALYSIS OF RDX WITH CONTAMINANTS

D.-J. Peng[1*], *C.-M. Chang*[1] *and M. Chiu*[2]

[1]Division of Occupational Safety, Institute of Occupational Safety and Health, Council of Labor Affairs, Executive Yuan, No. 99 Lane 407, Hengke Rd., Shijr City, Taipei, Taiwan 221, ROC
[2]Department of Occupational Safety and Hygiene, Tajen Institute of Technology, 20, Wei-Hsin Road, Yenpu Shiang, Pingtung Taiwan 907, ROC

Many investigations and researches studied the reaction ability between high explosive RDX and RDX with other chemicals. However, accidents still occur and operating problems exist among the RDX manufacturing process. This study utilized inherent safety concepts and DSC thermal analysis to assess the incompatible reaction hazards of RDX during usage, handling, storage, transporting and manufacturing. This assessment includes thermal curve observations and kinetic evaluations. A decomposition mechanism of the incompatible reaction is proposed. Among all the contaminants evaluated in this study, the existence of ferrous chloride tetrahydrate, ferric chloride hexahydrate and nitric acid shifted the main endothermic and exothermic reactions of RDX. These contaminants further advanced the exothermic temperature onset average by about 53, 46 and 61°C, respectively. The summarized results suggest that ferric oxide, ferrous chloride tetrahydrate, ferric chloride hexahydrate, acetone solution and nitric acid can influence the reaction and thermokinetic properties of RDX. These chemicals could induce potential hazards by causing temperature control instability, heating and cooling systems failure, and produce an unexpected secondary explosion. According to the conclusions of this study, potential incompatible RDX hazards during usage and manufacturing could be avoided.

Keywords: *contaminants, incompatible reaction hazards, inherent safety, RDX, thermal analysis*

Introduction

Based on past investigations and researches, nitrate reaction accidents occur primarily due to processes performed at temperatures close to the onset runaway reaction temperature (10 to 50°C less than the onset temperature) [1–4]. The main cause originates from operators who lack safety knowledge for this particular nitrate process. In addition, nitrate and its products, such as high explosives, lead to a great amount of unexpected heat release or some changes from the original reaction type, which incur faulty process performance and induce runaway reactions from contacting with contaminants like water, ferric ion, organic solvents and so on [5].

Nitrate high explosive RDX (1,3,5-trinitro-1,3,5-triazacyclohexane) often has opportunities to contact with contaminants during manufacturing, storage, transporting, usage and handling. For example, while an overdue shoot bomb is preparing to dismantle, it should be heated to melt the mixed (ex. TNT+RDX) or pure explosive (RDX). The rusty metal cartridge provides Fe_2O_3. Therefore, the dismantling operation which contains explosive and Fe_2O_3 under heating environment, creates potential hazards and has resulted in many accidents in the past. In addition, a great quantity of water is used as a coolant, thinner or reaction substance in the process. Thus, if RDX makes contact with sterilized chlorinated water, it has the chance to react with Fe_2O_3, $FeCl_2 \cdot 4H_2O$ and $FeCl_3 \cdot 6H_2O$ in pipes, or on the reactor walls and fixed valves. The products manufactured from RDX must be soaked in acetone solution to sieve the particle size and purify the products. Therefore, interactive reactions between RDX and the acetone solution could generate potential hazards and need to be identified. Nitric acid, the reactant in the RDX manufacturing process, could also make contact with RDX directly. It is necessary to investigate the incompatible effect of RDX and nitric acid contact.

The purpose of this study is to investigate the influences and potential hazards from RDX contacting with the chemicals/contaminants mentioned above. Recommendations and safety aspects will be introduced to the process operators to prevent incompatible reaction accidents. This study utilized thermal analysis techniques to analyze the incompatible effects of RDX and contaminants via thermal curves determination, thermal and kinetic parameter calculations and reaction mechanism evaluations. Hopefully, this work could reduce the incompatible reaction accidents caused by insufficient knowledge of the operators of the RDX processing reaction properties and potential hazards.

* Author for correspondence: Deng@mail.iosh.gov.tw

1388–6150/$20.00

Akadémiai Kiadó, Budapest, Hungary
Springer, Dordrecht, The Netherlands

Experimental

High explosive RDX

Pure RDX was provided directly from the manufacturer. The RDX has highly stable chemical properties with large heat release. The sample mass of pure RDX ranged between 1.5±0.1 mg.

Contaminants

Ferric oxide (>99.0 mass%), ferrous chloride tetrahydrate (15.0 mass%), ferric chloride hexahydrate (40.0 mass%) and acetone (100.0 mass%) were purchased from Merck and Co. Inc. The nitric acid (100.0 mass%) used to produce RDX in the actual process was provided by the manufacturer. The contaminant sample masses used were between 1.5±0.1 mg.

Instruments

Incompatible reaction determination was conducted using the Mettler Toledo DSC 822^e differential scanning calorimeter. Test samples were put in a high pressure gold-plated steel crucible, which contained 40 μL and was hermetically sealed under ambient atmosphere by a top lid. This closed crucible could endure maximum pressure of 15 MPa. The heating rates used in the dynamic scanning experiments were 1, 2, 4 and 10°C min^{-1} to calculate the RDX and contaminant reaction heat, thermal curves, activity energy and frequency factors.

Results and discussion

This study investigates the potential incompatible reaction hazards caused by the following contaminants: Fe_2O_3, $FeCl_2{\cdot}4H_2O$, $FeCl_3{\cdot}6H_2O$, CH_3COCH_3 and HNO_3. A DSC thermal curves comparison and kinetics determination were performed at heating rates of 1, 2, 4 and 10°C min^{-1}. The DSC experimental data for pure RDX and contaminants are shown in Table 1. Accordingly, the heating rate influence was considered in the incompatible experiments. The following sections will discuss the RDX incompatible reaction phenomena and the effects of a variety of heating rates.

Ferric oxide+RDX

From the DSC thermal curves, Fe_2O_3 led the original endothermic phase transition of RDX disappeared, changed the main exothermic peak from two similar plateau exothermic peaks to a strong and sharp peak. This change is shown in Fig. 1. It can also be observed that the maximum heat flow of RDX had

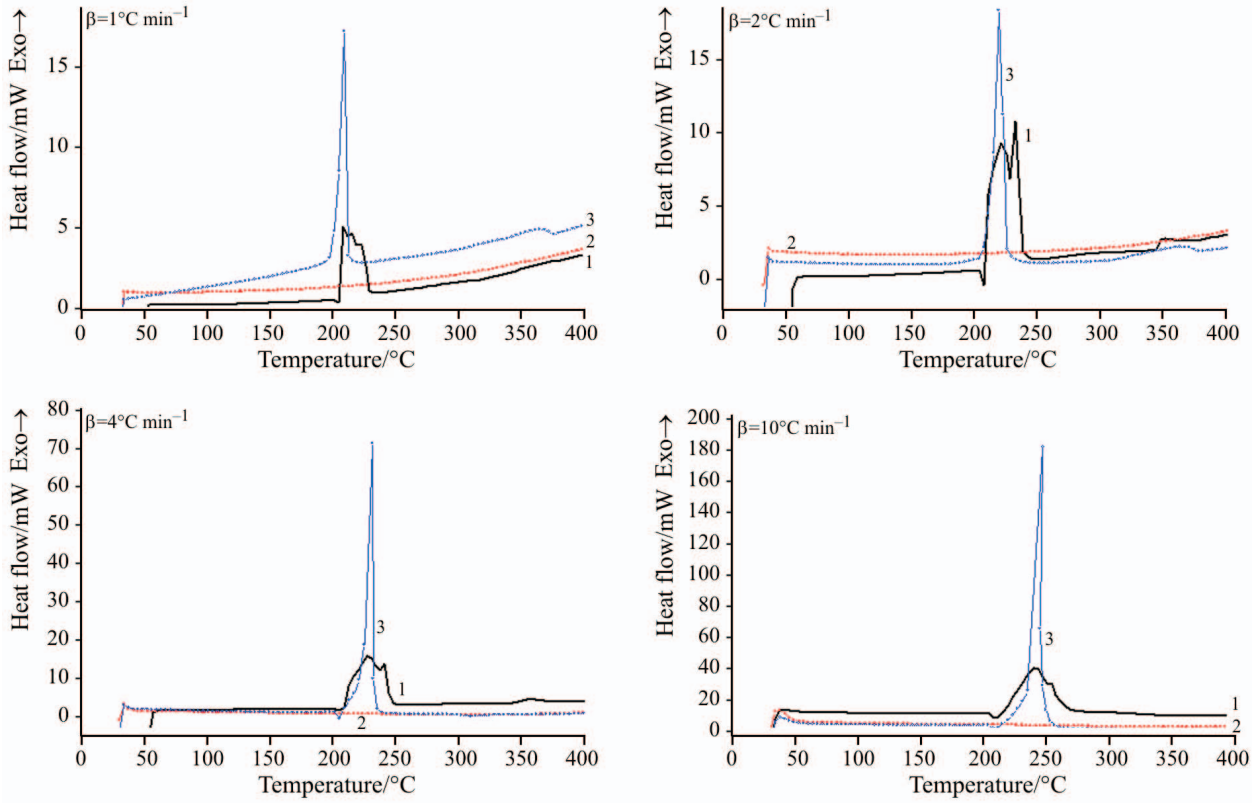

Fig. 1 Heat flow *vs*. temperature plot for DSC dynamic experiments of RDX mixed with ferric oxide at scanning rate 1, 2, 4 and 10°C min^{-1}; curve 1 – RDX, curve 2 – Fe_2O_3 and curve 3 – RDX+Fe_2O_3

changed from 7.78~29.81 mW (at various heating rate) to 14.39~180.63 mW. Despite ferric oxide causing the RDX heat release to decrease, the maximum heat flow enhanced with the heating rate increased and delayed the exothermic temperature onset, as presented in Table 2.

Table 1 Summarized results for DSC experiments of pure RDX and contaminants

β/°C min^{-1}	*m*/mg	Endothermic peaks							
		$T_{0.1}$/°C	ΔH_1/J g^{-1}	$T_{0.2}$/°C	ΔH_2/J g^{-1}	$T_{0.3}$/°C	ΔH_3/J g^{-1}	$T_{0.4}$/°C	ΔH_4/J g^{-1}
1	RDX 1.52	204.949	–92.161	–	–	–	–	–	–
	Fe_2O_3 1.51	–	–	–	–	–	–	–	–
	$FeCl_2{\cdot}4H_2O$ 1.52	76.312	–63.716	233.603	–1.706	292.048	–51.147	306.451	–188.606
	$FeCl_3{\cdot}6H_2O$ 1.51	33.163	–94.248	297.011	–354.813	–	–	–	–
	CH_3COCH_3 1.53	–	–	–	–	–	–	–	–
	HNO_3 1.55	295.774	–33.329	–	–	–	–	–	–
2	RDX 1.53	205.355	–93.757	–	–	–	–	–	–
	Fe_2O_3 1.50	–	–	–	–	–	–	–	–
	$FeCl_2{\cdot}4H_2O$ 1.50	76.739	–95.452	238.174	–27.404	317.532	–21.013	351.410	–163.789
	$FeCl_3{\cdot}6H_2O$ 1.52	33.549	–55.446	321.867	–291.604	–	–	–	–
	CH_3COCH_3 1.51	–	–	–	–	–	–	–	–
	HNO_3 1.51	99.931	–26.603	124.012	–47.956	171.092	–553.204	–	–
4	RDX 1.50	205.556	–73.504	–	–	–	–	–	–
	Fe_2O_3 1.51	–	–	–	–	–	–	–	–
	$FeCl_2{\cdot}4H_2O$ 1.50	78.652	–76.049	236.217	–13.118	283.567	–45.449	354.983	–147.457
	$FeCl_3{\cdot}6H_2O$ 1.51	34.293	–39.664	283.762	–503.238	–	–	–	–
	CH_3COCH_3 1.48	–	–	–	–	–	–	–	–
	HNO_3 1.52	186.791	–155.436	239.080	–66.383	–	–	–	–
10	RDX 1.48	210.062	–63.450	–	–	–	–	–	–
	Fe_2O_3 1.51	–	–	–	–	–	–	–	–
	$FeCl_2{\cdot}4H_2O$ 1.55	82.256	–84.513	240.001	–6.105	366.654	–172.582	–	–
	$FeCl_3{\cdot}6H_2O$ 1.56	37.168	–6.933	325.181	–268.572	379.027	–4.374	–	–
	CH_3COCH_3 1.51	–	–	–	–	–	–	–	–
	HNO_3 1.49	168.511	–9.622	203.334	–147.867	247.243	–19.568	270.820	–14.611

β/°C min^{-1}	*m*/mg	Exothermic peaks					
		$T_{0.1}$/°C	ΔH_1/J g^{-1}	$T_{0.2}$/°C	ΔH_2/J g^{-1}	$T_{0.3}$/°C	ΔH_3/J g^{-1}
1	RDX 1.52	221.782	3185.783	–	–	–	–
	Fe_2O_3 1.51	–	–	–	–	–	–
	$FeCl_2{\cdot}4H_2O$ 1.52	–	–	–	–	–	–
	$FeCl_3{\cdot}6H_2O$ 1.51	–	–	–	–	–	–
	CH_3COCH_3 1.53	285.303	300.010	–	–	–	–
	HNO_3 1.55	177.018	355.251	300.786	153.668	–	–
2	RDX 1.53	228.248	4001.887	–	–	–	–
	Fe_2O_3 1.50	–	–	–	–	–	–
	$FeCl_2{\cdot}4H_2O$ 1.50	–	–	–	–	–	–
	$FeCl_3{\cdot}6H_2O$ 1.52	–	–	–	–	–	–
	CH_3COCH_3 1.51	169.304	2.653	261.409	134.903	365.568	15.164
	HNO_3 1.51	282.682	94.544	–	–	–	–
4	RDX 1.50	208.242	3677.549	–	–	–	–
	Fe_2O_3 1.51	–	–	–	–	–	–
	$FeCl_2{\cdot}4H_2O$ 1.50	–	–	–	–	–	–
	$FeCl_3{\cdot}6H_2O$ 1.51	–	–	–	–	–	–
	CH_3COCH_3 1.48	94.867	2.029	174.127	31.522	272.512	29.532
	HNO_3 1.52	321.927	550.118	–	–	–	–
10	RDX 1.48	219.154	3636.690	–	–	–	–
	Fe_2O_3 1.51	–	–	–	–	–	–
	$FeCl_2{\cdot}4H_2O$ 1.55	–	–	–	–	–	–
	$FeCl_3{\cdot}6H_2O$ 1.56	–	–	–	–	–	–
	CH_3COCH_3 1.51	100.047	4.5062	184.511	142.502	282.164	37.5347
	HNO_3 1.49	327.628	439.634	–	–	–	–

Table 2 Summarized results for DSC experiments of ferric oxide mixed with RDX

Sample	β/°C min^{-1}	*m*/mg	$T_{0,endo}$/°C	ΔH_{endo}/J g^{-1}	$T_{0,exo}$/°C	$T_{p,exo}$/°C	Φ_{max}/mW	ΔH_{exo}/J g^{-1}
RDX+Fe_2O_3	1	RDX: 1.50 Fe_2O_3: 1.47	–	–	203.982	209.338	14.388	1439.662
RDX+Fe_2O_3	2	RDX: 1.52 Fe_2O_3: 1.52	202.553	–28.201	214.853	220.364	27.687	1628.689
RDX+Fe_2O_3	4	RDX: 1.48 Fe_2O_3: 1.50	204.260	–31.167	228.308	235.882	173.644	2100.484
RDX+Fe_2O_3	10	RDX: 1.5 Fe_2O_3: 1.51	209.166	–23.549	242.148	250.612	180.617	2026.333

Ferrous chloride tetrahydrate+RDX

The endothermic phase transition disappeared at 1, 2 and 4°C min^{-1} heating rates while ferrous chloride tetrahydrate contacted with RDX, as shown in Fig. 2. The ferrous chloride tetrahydrate self-endothermic phenomenon occurred (75.51~82.49°C) in all thermal curves at various heating rates. Also, ferrous chloride tetrahydrate would lead to the RDX reaction temperature onset advanced about 53°C, from 208.24~228.25 to 157.49~177.83°C. The shape of the main exothermic peak has changed from two peaks adjacent to each other to a gradual and smooth slope. The summarized experimental results are presented in Table 3. The ferrous chloride tetrahydrate caused both the amount of heat release and maximum heat flow to reduce. Furthermore, the reaction curve after the main exothermic peak presented a baseline that gradually increased with temperature went up. The heat capacity of these mixtures had changed.

Ferric chloride hexahydrate+RDX

Ferric chloride hexahydrate caused the high explosive RDX endothermic transition phase to disappear and advanced the exothermic temperature onset from 208.24~228.25 to 158.02~187.50°C, approximately 46°C decrease as shown in Table 4. It also changed the shape of the exothermic peak into a smoother curve, as presented in Fig. 3. After the main heat release under heating rates 1 and 4°C min^{-1}, the thermal curves showed a ferric chloride hexahydrate self-endothermic phase transition phenomenon. At various heating rates, the incompatible reaction behaviors of

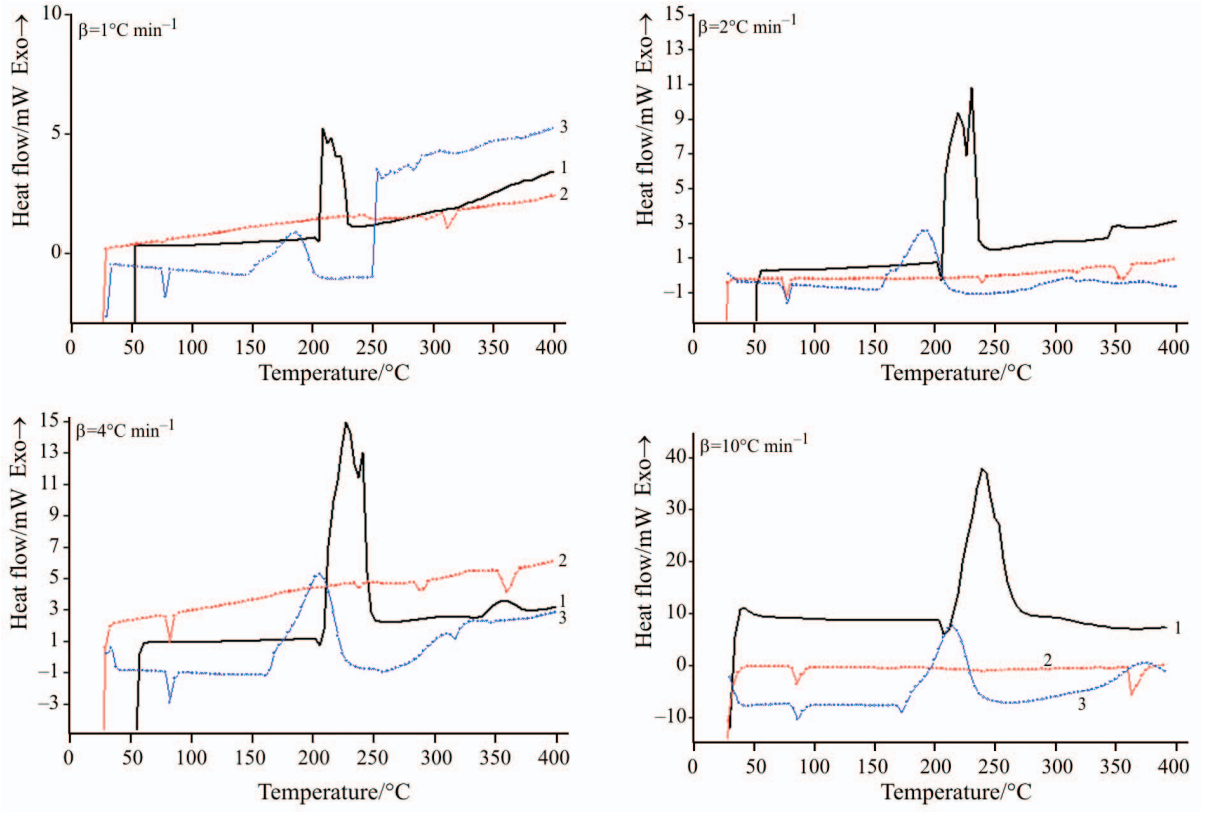

Fig. 2 Heat flow *vs*. temperature plot for DSC dynamic experiments of RDX mixed with ferrous chloride tetrahydrate at scanning rate 1, 2, 4 and 10°C min^{-1}; curve 1 – RDX, curve 2 – $FeCl_2$ and curve 3 – RDX+$FeCl_2$

Table 3 Summarized results for DSC experiments of ferrous chloride tetrahydrate mixed with RDX

Sample	β/°C min^{-1}	*m*/mg	$T_{0,endo,1}$/°C	$\Delta H_{endo,1}$/J g^{-1}	$T_{0,exo}$/°C	$T_{p,exo}$/°C	Φ_{max}/mW	ΔH_{exo}/J g^{-1}	$T_{0,endo,2}$/°C	$\Delta H_{endo,2}$/J g^{-1}
RDX+$FeCl_2 \cdot 4H_2O$	1	RDX: 1.49 $FeCl_2 \cdot 4H_2O$: 1.51	76.591	–41.092	168.882	185.747	1.864	1172.163	282.677	–74.807
RDX+$FeCl_2 \cdot 4H_2O$	2	RDX: 1.52 $FeCl_2 \cdot 4H_2O$: 1.50	75.510	–48.581	161.233	192.492	3.577	1128.324	314.051	–64.839
RDX+$FeCl_2 \cdot 4H_2O$	4	RDX: 1.47 $FeCl_2 \cdot 4H_2O$: 1.51	80.183	–39.177	157.488	206.062	6.238	1136.829	314.980	–20.459
RDX+$FeCl_2 \cdot 4H_2O$	10	RDX: 1.48 $FeCl_2 \cdot 4H_2O$: 1.50	82.486	–40.929	177.828	217.374	15.284	1063.212	172.393	–11.270

Table 4 Summarized results for DSC experiments on ferric chloride hexahydrate mixed with RDX

Sample	β/°C min^{-1}	*m*/mg	$T_{0,exo}$/°C	$T_{p,exo}$/°C	Φ_{max}/mW	ΔH_{exo}/J g^{-1}	$T_{0,endo}$/°C	ΔH_{endo}/J g^{-1}
RDX+$FeCl_3 \cdot 6H_2O$	1	RDX: 1.52 $FeCl_3 \cdot 6H_2O$: 1.47	158.021	191.782	2.207	1052.689	258.264	–196.291
RDX+$FeCl_3 \cdot 6H_2O$	2	RDX: 1.49 $FeCl_3 \cdot 6H_2O$: 1.51	176.432	199.102	4.567	1213.112	–	–
RDX+$FeCl_3 \cdot 6H_2O$	4	RDX: 1.51 $FeCl_3 \cdot 6H_2O$: 1.50	173.123	208.514	9.964	1551.124	312.913	–34.427
RDX+$FeCl_3 \cdot 6H_2O$	10	RDX: 1.51 $FeCl_3 \cdot 6H_2O$: 1.50	187.508	220.448	19.207	1382.518	–	–

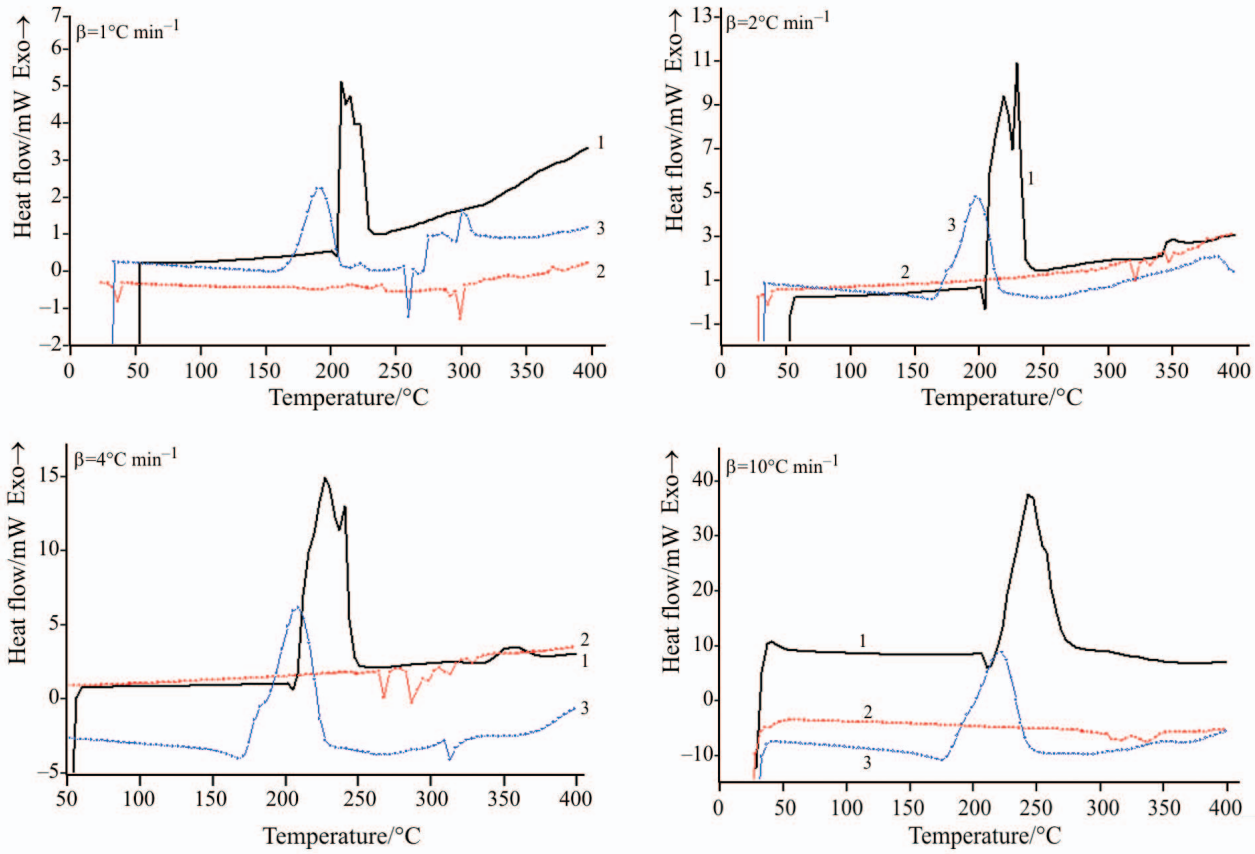

Fig. 3 Heat flow *vs*. temperature plot for DSC dynamic experiments of RDX mixed with ferric chloride hexahydrate at scanning rate 1, 2, 4 and 10°C min^{-1}; curve 1 – RDX, curve 2 – $FeCl_3$ and curve 3 – RDX+$FeCl_3$

RDX contact with ferric chloride hexahydrate were different from pure RDX. The amount of heat released was less than that of pure RDX, and the maximum heat flow increased, and it would result in different potential hazards.

Acetone solution+RDX

The acetone solution, used as a crystal soaking solvent, in contact with RDX could cause the RDX endothermic phase transition to disappear. The amount of heat released is reduced and the maximum heat flow is increased when the heating rate is increased. The exothermic reaction is also shifted from two similar plateau peaks into a strong and sharp peak. Acetone solution offers no protons in this reaction because it is an oxidizing agent. The incompatible effects could still occur because acetone solution, an oxidant, could release oxygen and accelerates the pyrolysis decomposition of RDX when heat is added. The summarized experimental results and thermal curves are shown in Table 5 and Fig. 4.

Nitric acid+RDX

The manufacturing reactant nitric acid could cause the endothermic phase transition in RDX to disappear at heating rates of 1, 2 and 4°C min^{-1}. Heat release of nitric acid produce a gradual plateau peak and leads the onset exothermic temperature to advance to about 52°C, as shown in Table 6 and Fig. 5. After the main exothermic peak, the thermal curve presented an unstable endothermic peak. Preliminary, as observed from the thermal curves of Fig. 5, this endothermic peak belongs to reaction property of nitric acid. However, intermediate products produced after the main exothermic reaction of RDX and nitric acid mixture might be another possibility to explain this phenomenon. This phenomenon could cause potential unstable hazards which require further study to understand [6].

Kinetics evaluations

Because the main RDX-contaminant exothermic peak corresponds to contaminant reactions with a synergetic heat release, the kinetic parameters videlicet, activation energy, E_a and frequency factor, A of the reaction, for these reactions were evaluated. The Kissinger and Ozawa methods were employed to analyze DSC experimental data in Tables 2 to 6 at heating rates of 1, 2, 4 and 10°C min^{-1}.

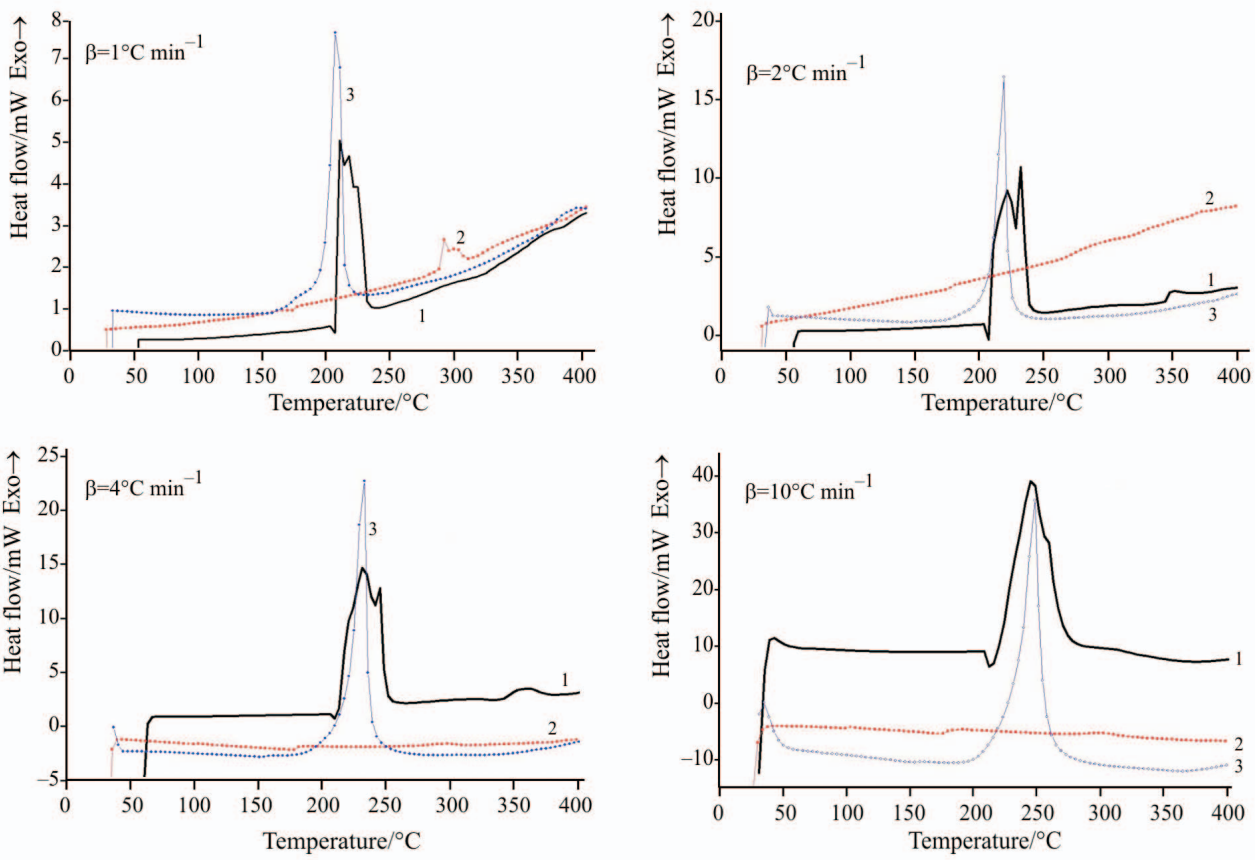

Fig. 4 Heat flow *vs*. temperature plot for DSC dynamic experiments of RDX mixed with acetone solution at scanning rate 1, 2, 4 and 10°C min^{-1}; curve 1 – RDX, curve 2 – CH_3COCH_3 and curve 3 – RDX+CH_3COCH_3

Table 5 Summarized results for DSC experiments on acetone solution mixed with RDX

Sample	β/°C min^{-1}	*m*/mg	$T_{0,exo}$/°C	$T_{p,exo}$/°C	Φ_{max}/mW	ΔH_{exo}/J g^{-1}
RDX+CH_3COCH_3	1	RDX: 1.51 acetone: 1.50	197.683	207.508	8.328	1593.978
RDX+CH_3COCH_3	2	RDX: 1.49 acetone: 1.50	207.070	217.463	15.804	1796.047
RDX+CH_3COCH_3	4	RDX: 1.52 acetone: 1.53	217.486	228.122	27.872	1867.434
RDX+CH_3COCH_3	10	RDX: 1.49 acetone: 1.51	232.337	246.071	45.912	1863.486

Kissinger method [7–10]

The Kissinger method is based on the plot of $\ln(\beta / T_p^2)$ *vs*. $-1 / T_p$, where β is the heating rate and T_p the DSC absolute peak temperature. The activity energy and frequency factor values were calculated from Kissinger's plot with the equation as follows:

$$\ln\left(\frac{\beta}{T_p^2}\right) = \ln\left(\frac{AR}{T}\right) - \frac{E_a}{RT_p} \qquad (1)$$

Ozawa method [11–14]

The Ozawa method uses the plot of logβ *vs*. $-1/T_p$. The kinetic parameters are obtained from Eq. (2) which has item:

$$G(x_m) = \frac{ART_p^2}{\beta E_a}\exp\left(-\frac{E_a}{RT_p}\right)$$

$$\log\beta = -0.4567\frac{E_a}{RT_p} - \qquad (2)$$

$$-2.315 + \log\frac{AE_a}{R} - \log G(x_m)$$

Table 6 Summarized results for DSC experiments on nitric acid mixed with RDX

Sample	β/°C min^{-1}	m/mg	$T_{0,endo,1}$/°C	$\Delta H_{endo,1}$/J g^{-1}	$T_{0,exo}$/°C	$T_{p,exo}$/°C	Φ_{max}/mW	ΔH_{exo}/J g^{-1}	$T_{0,endo,2}$/°C	$\Delta H_{endo,2}$/J g^{-1}
RDX+HNO_3	1	RDX: 1.51 HNO_3: 1.55	–	–	146.403	179.707	2.417	2148.191	282.402	–10.207
RDX+HNO_3	2	RDX: 1.49 HNO_3: 1.49	–	–	158.744	195.391	5.559	2921.892	238.842	–200.364
RDX+HNO_3	4	RDX: 1.48 HNO_3: 1.49	–	–	158.749	211.030	11.946	3307.923	274.784	–8.937
RDX+HNO_3	10	RDX: 1.47 HNO_3: 1.50	113.538	–4.584	169.202	224.053	26.360	2851.418	294.368	–36.338

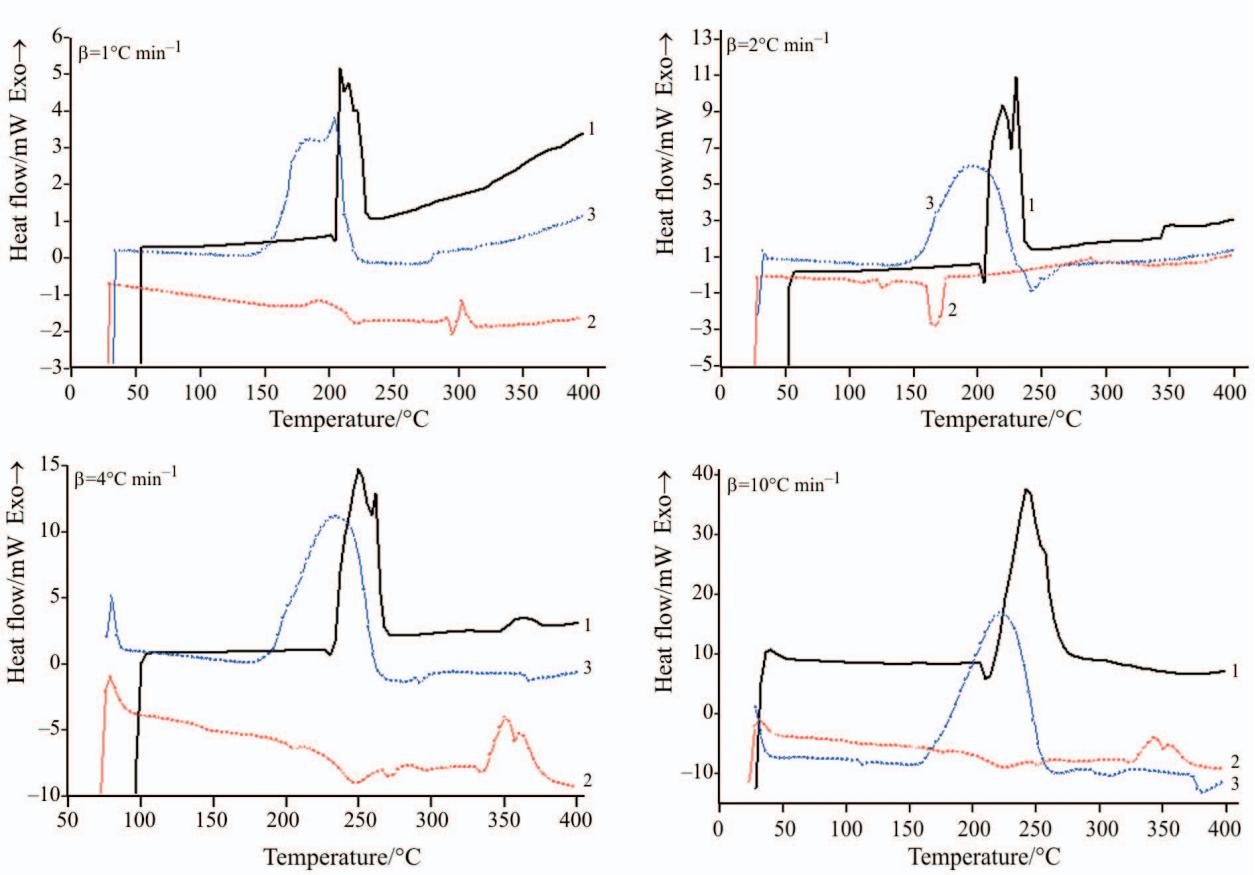

Fig. 5 Heat flow *vs*. temperature plot for DSC dynamic experiments of RDX mixed with nitric acid at scanning rate 1, 2, 4 and 10°C min^{-1}; curve 1 – RDX, curve 2 – HNO_3 and curve 3 – RDX+HNO_3

Eventually, the RDX with contaminant kinetic parameters are presented in Table 7. Both the activation energies and frequency factors of RDX with contaminant decreased compared to pure RDX. This means that when RDX is in contact with a variety of contaminants, the reaction kinetic types could incur substantial changes, produce unstable conditions and increase the opportunity for explosion. Incompatible RDX contaminant reactions change the reaction type, such as the shape of the exothermic peak, etc.

Proposed reaction mechanisms

The RDX decomposition paths have been widely investigated over the past couple decades [15–21]. Among these researches, Zhao *et al*., suggested that the collision-free decomposition of RDX follows at least two different reaction channels, ionic reaction and pyrolysis decomposition paths, as shown in Fig. 6 [10, 15]. In addition, Rogers and Bulusu indicated that the rupture of the C–H bond controls the rate of RDX first order kinetic decomposition [22, 23].

Ferric oxide and acetone solution could not provide a proton to produce an ionic reaction in this study. They are both oxidants that could release oxygen via heat to accelerate the pyrolysis decomposition and it would cause less influence with increasing heating rate. This could also be observed from the shifted exothermic temperature onset. The proposed pyrolysis decomposition mechanism is shown in Fig. 7.

Primarily, the Fe^{2+} would become Fe^{3+} through an oxidation reaction. The ferrous chloride tetrahydrate and ferric chloride hexahydrate would then produce similar pyrolysis and ionic reaction steps, as shown in Figs 7 and 8. The pyrolysis reaction occurs due to the basic RDX reaction ability. The RDX ionic reaction presented in Fig. 6 initially breaks the N–NO_2 bond. The reaction pathway is varied via H_2O^+ which is decomposed from ferric chloride hexahydrate and provides a positive ion. The reaction products are 1,3,5-triazine and HNO_2.

Despite nitric acid being an oxidant, it could also react in both pyrolysis and ionic reactions, as demonstrated in Figs 7 and 9. The pyrolysis reaction is caused by rapid RDX decomposition. In the proposed ionic reaction decomposition path, nitric acid first has an interactive reaction with water to generate charged ions NO_3^- and H_3^+O which would continuously affect the respective RDX C–H and NO–O bonds. The reaction products are also 1,3,5-triazine and HNO_2, the same as the results from ferrous chloride tetrahydrate and ferric chloride hexahydrate.

Table 7 Calculated RDX kinetic parameters with contaminants

Sample	Kissinger method			Ozawa method		
	E_a/kJ mol^{-1}	A/s^{-1}	γ	E_a/kJ mol^{-1}	A/s^{-1}	γ
pure RDX	176.7307	$8.9326\cdot10^{14}$	0.9999	176.4818	$1.4259\cdot10^{15}$	0.9999
Fe_2O_3+RDX	106.0368	$8.1989\cdot10^{7}$	0.9934	108.7355	$1.8384\cdot10^{8}$	0.9944
$FeCl_2$+RDX	121.4925	$2.0232\cdot10^{10}$	0.9842	123.2646	$4.0923\cdot10^{10}$	0.9865
$FeCl_3$+RDX	143.3250	$3.6102\cdot10^{12}$	0.9985	144.0832	$6.2979\cdot10^{12}$	0.9986
CH_3COCH_3+RDX	115.5729	$1.0275\cdot10^{9}$	0.9966	117.7031	$2.0889\cdot10^{9}$	0.9970
HNO_3+RDX	99.5851	$6.4686\cdot10^{7}$	0.9918	102.3567	$1.5301\cdot10^{8}$	0.9931

γ – correction coefficient for linear regression

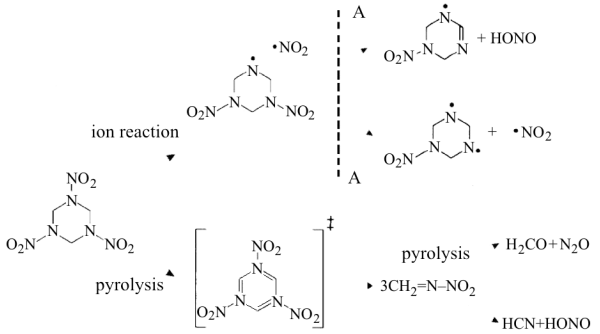

Fig. 6 Proposed RDX decomposition paths [21]

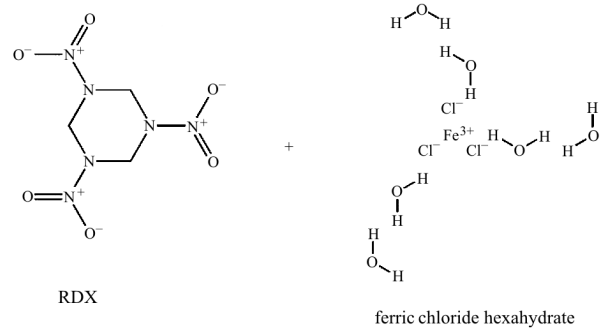

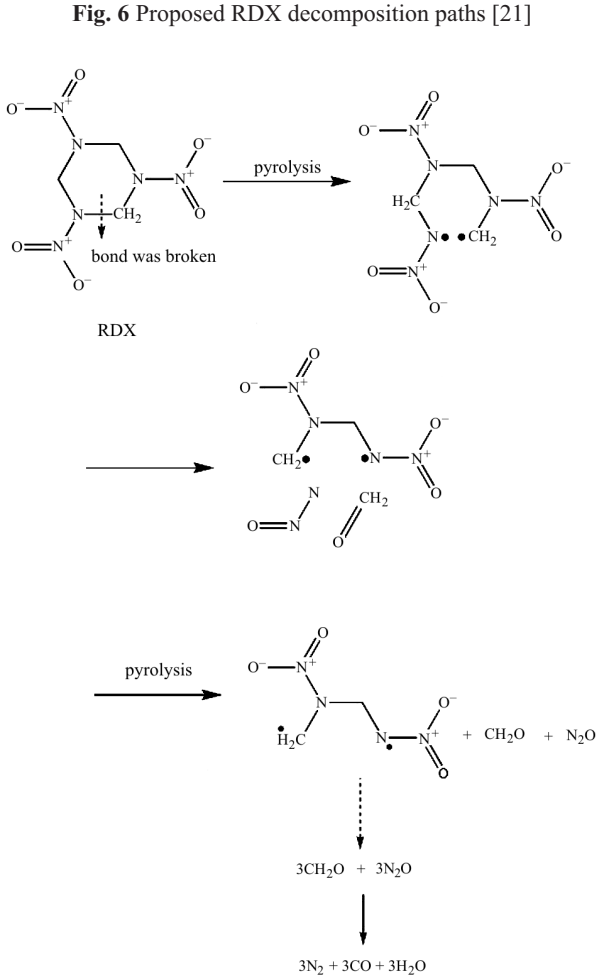

Fig. 7 Proposed overall kinetic pyrolysis mechanism of RDX

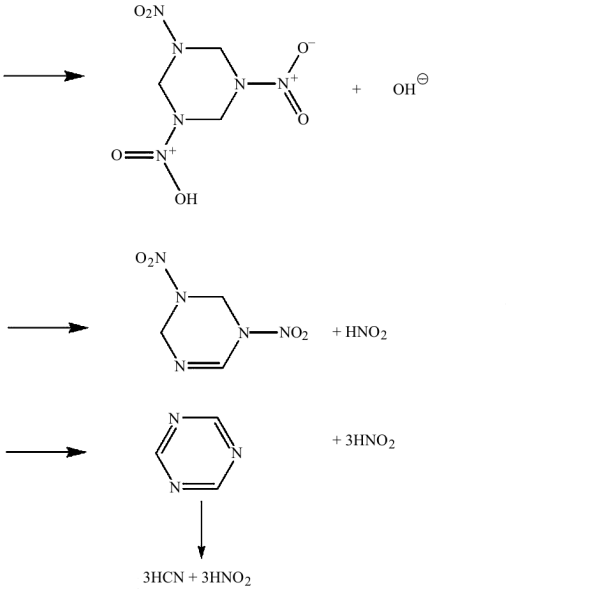

Fig. 8 Proposed overall kinetic decomposition mechanism of RDX mixed with ferric chloride hexahydrate

To understand the RDX contaminant incompatibility effects in more detail, this study proposed the aforementioned pyrolysis and ionic decomposition paths based on past investigations as shown in Fig. 6 [21]. However, all of the aforementioned reaction pathways need further verification using analysis instruments, such as GC (gas chromatography), HPLC (high performance liquid chromatography) and so on. These results will present in the future [6].

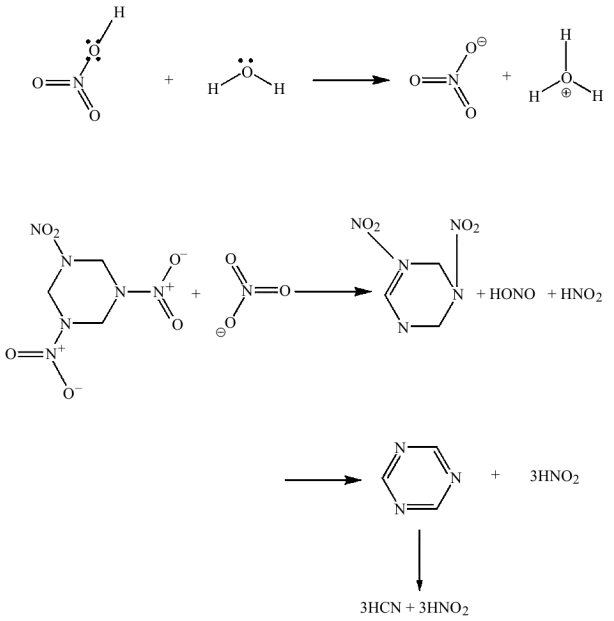

Fig. 9 Proposed overall kinetic decomposition mechanism of RDX mixed with nitric acid

Conclusions

Based on the DSC experimental results, kinetic evaluations, proposed reaction mechanisms and the above discussions, high explosive RDX in contact with ferric oxide, ferrous chloride tertrahydrate, ferric chloride hexahydrate, acetone solution and nitric acid, produce changes in the thermokinetic properties and decomposition mechanisms. Thus, potential incompatible RDX contaminate hazards during manufacturing and usage must be prevented according to the following findings:

- All contaminants used in this study induced the RDX endothermic peak to disappear and shifted the main exothermic peak profile. Ferrous chloride tetrahydrate and ferric chloride hexahydrate further produced an endothermic reaction. Attention must be paid to these phenomena because of potential hazards from the incompatible temperature control, heating and cooling systems failure, which may produce an unexpected explosion. This is a serious potential hazard.
- The thermodynamic properties (ex. T_0, T_f, $\dot{Q}_{max}$ and ΔH, etc.), kinetic parameters (ex. E_a and A) and reaction pathways exhibited significant changes after RDX was mixed with ferric oxide, ferrous chloride tetrahydrate, ferric chloride hexahydrate, acetone solution and nitric acid.

Hopefully, this study will further understand the incompatible risks involved in contaminated RDX during production, handling, transporting and storage.

Nomenclature

A	frequency factor for pure RDX or RDX mixed with contaminants reaction/s^{-1}
E_a	activation energy of pure RDX or RDX mixed with contaminants reaction/kJ mol^{-1}
ΔH	enthalpy reaction differences/kJ mol^{-1}
ΔH_1	enthalpy difference at reaction temperature 1/kJ mol^{-1}
ΔH_2	enthalpy difference at reaction temperature 2/kJ mol^{-1}
ΔH_3	enthalpy difference at reaction temperature 3/kJ mol^{-1}
m	sample mass/mg
$\dot{Q}_{max}$	maximum heat flow of DSC thermal curves/mW
β	heating rate of DSC experiment/°C min^{-1}
γ	correction coefficient for linear regression/dimensionless
R	universal gas constant/J mol^{-1} K^{-1}
T	temperature of reaction in DSC experiment/°C or K
T_0	onset reaction temperature/°C or K
T_1	reaction temperature 1 of DSC dynamic test/°C or K
T_2	reaction temperature 2 of DSC dynamic test/°C or K
T_3	reaction temperature 3 of DSC dynamic test/°C or K
T_p	peak temperature in DSC thermal curves/°C or K

Subscripts

1	condition in reaction 1
2	condition in reaction 2
3	condition in reaction 3
4	condition in reaction 4
endo	endothermic reaction
exo	exothermic reaction

Acknowledgements

The authors appreciate the support provided by The Institute of Occupational Safety and Health, Council of Labor Affairs, Executive Yuan, under grant No. IOSH93-S302, 203Rd Arsenal Material Production Service, Dr. Kwan-Hua Hu who provided valuable help in this study and Ms. Ching-Weng Young for assisting the experiments.

References

1 T. L. Davis, Chemistry of Powder and Explosives, Wiley, New York, USA 1943.
2 R. E. Kirk and D. F. Othemer, Encyclopaedia of Chemical Technology, 4th Edition, John Wiley and Sons, Inc., New York, USA 1998.
3 B. Pantex, DOE Explosives Safety Manual-Pantex Version, Department of Energy, USA 1998.
4 F. P. Lees, Loss Prevention in the Process Industries, 2nd Edition, Butterworth Heinemann, Oxford UK, 2001.
5 D. J. Peng, C. M. Chang and M. Chiu, J. Hazard. Mater., A, 114 (2004) 1.

6 D. J. Peng and C. M. Chang, J. Phys. Chem. B, (in preparation-title as 'Decomposition Mechanism Study of RDX with Contaminants').
7 H. E. Kissinger, Anal. Chem., 29 (1957) 1703.
8 A. Mianowski and R. Bigda, J. Therm. Anal. Cal., 75 (2004) 355.
9 T. L. Shanker Rao, K. N. Lad and A. Pratap, J. Therm. Anal. Cal., 78 (2004) 769.
10 R. Lopez-Fonseca, I. Landa, M. A. Gutierrez-Ortiz and J. R. Gonzalez-Velasco, J. Therm. Anal. Cal., 80 (2005) 65.
11 T. Ozawa, J. Thermal Anal., 2 (1970) 301.
12 J. A. F. F. Rocco, J. E. S. Lima, A. G. Frutuoso, K. Iha, M. Ionashiro, J. R. Matos and M. E. V. Suárez-Iha, J. Therm. Anal. Cal., 75 (2004) 551.
13 C. Korah Bina, K. G. Kannan and K. N. Ninan, J. Therm. Anal. Cal., 78 (2004) 753.
14 P. Thomas and P. Šimon, J. Therm. Anal. Cal., 80 (2005) 77.
15 J. Yinon, R. A. Yost and S. Bulusu, J. Chromatogr. A, 688 (1994) 231.
16 H. Osmark, H. Bergman, K. Ekvall and A. Langlet, Thermochim. Acta, 260 (1995) 201.
17 G. Hussain and G. J. Rees, Fuel, 74 (1995) 273.
18 E. S. Kim, H. S. Lee, C. F. Mallery and S. T. Thynell, Combust. Flame, 110 (1997) 239.
19 M. A. Bohn, R. Schweppe and W. Weisweiler, Waste Manage., 17 (1997) 175.
20 C. A. Groom, S. Beaudet, A. Halasz, L. Paquet and J. Hawari, J. Chromatogr. A, 909 (2001) 53.
21 X. Zhao, E. J. Hintsa and Y. T. Lee, J. Chem. Phys., 88 (1988) 801.
22 S. L. Rogers, M. B. Coolidge, W. J. Lauerdale and S. A. Shackelford, Thermochim. Acta, 177 (1991) 151.
23 S. Bulusu, D. I. Weinstein, J. R. Autera and R. W. Velicky, J. Phys. Chem., 90 (1986) 4121.

Received: August 13, 2005
Accepted: November 10, 2005

DOI: 10.1007/s10973-005-6961-8